Proc. Natl. Acad. Sci. USA
Vol. 93, pp. 8368–8373, August 1996
Cell Biology

Ultraviolet-induced movement of the human DNA repair protein, *Xeroderma pigmentosum* type G, in the nucleus

(nucleotide excision repair/nuclear matrix/immunofluorescence/ultraviolet damage)

MIN S. PARK*†, JEFFREY A. KNAUF*‡, STEPHANIE H. PENDERGRASS, CHRISTOPHER H. COULON, GARY. F. STRNISTE, BABETTA L. MARRONE, AND MARK A. MACINNES

Life Sciences Division, Los Alamos National Laboratory, Los Alamos, NM 87545

Communicated by Stirling A. Colgate, Los Alamos National Laboratory, Los Alamos, NM, April 17, 1996 (received for review May 12, 1995)

ABSTRACT ***Xeroderma pigmentosum* type G (XPG) is a human genetic disease exhibiting extreme sensitivity to sunlight. XPG patients are defective XPG endonuclease, which is an enzyme essential for DNA repair of the major kinds of solar ultraviolet (UV)-induced DNA damages. Here we describe a novel dynamics of this protein within the cell nucleus after UV irradiation of human cells. Using confocal microscopy, we have localized the immunofluorescent, antigenic signal of XPG protein to foci throughout the cell nucleus. Our biochemical studies also established that XPG protein forms a tight association with nuclear structure(s). In human skin fibroblast cells, the number of XPG foci decreased within 2 h after UV irradiation, whereas total nuclear XPG fluorescence intensity remained constant, suggesting redistribution of XPG from a limited number of nuclear foci to the nucleus overall. Within 8 h after UV, most XPG antigenic signal was found as foci. Using β-galactosidase–XPG fusion constructs (β-gal–XPG) transfected into HeLa cells, we have identified a single region of XPG that is evidently responsible both for foci formation and for the UV dynamic response. The fusion protein carrying the C terminus of XPG (amino acids 1146–1185) localized β-gal specific antigenic signal to foci and to the nucleolus regions. After UV irradiation, antigenic β-gal translocated reversibly from the subnuclear structures to the whole nucleus with kinetics very similar to the movements of XPG protein. These findings lead us to propose a model in which distribution of XPG protein may regulate the rate of DNA repair within transcriptionally active and inactive compartments of the cell nucleus.**

Solar ultraviolet radiation (UV) is recognized as an increasingly important risk to health from cellular DNA damage, including an ongoing epidemic of skin carcinogenesis in certain human populations. The biochemical pathway of nucleotide excision repair (NER) is the primary mechanism in mammalian cells to remove a wide variety of DNA photo-lesions and chemical adducts (for review, see ref. 1). Eukaryotic NER produces excision of a damaged oligonucleotide of ≈29 bp followed by gap-filling DNA synthesis (2, 3). Surprisingly, cyclobutane-pyrimidine photodimers, a major cytotoxic and mutagenic class of solar UV lesions, are repaired with different kinetics depending on their location in the genome (for review, see refs. 4 and 5). Actively transcribed genes in rodent and humans cells exhibit a rapid NER of pyrimidine dimers, whereas their removal from inactive nuclear regions is several-fold slower (6, 7). Transcriptional coupling of NER may be facilitated by a direct interaction of RNA Polymerase II transcription complex(es), in particular the TFIIH complex, with lesions. In fact, several essential NER enzymes are integral components of TFIIH (8–10). Consistent with the transcription coupling model, cellular immunofluorescence studies have indicated colocalization of nascent RNA transcripts with foci of NER related DNA synthesis at early times after relatively high UV doses (11). Furthermore, we show here that a key NER enzyme displays spatial and temporal regulations of its distribution within the nucleus architecture after moderate UV doses.

In recent decades, there has been substantial progress in understanding the basic structure of the cell nucleus and its implications in functional compartmentation (12). A proteinaceous framework known as the nuclear matrix or scaffold has been implicated in a variety of nuclear processes including DNA replication (13), excision repair (14, 15), and RNA transcription and processing (16–18). There is good evidence that regulatory proteins are situated near to the attachment sites of DNA loops to the nuclear matrix (19, 20). This type of geometrical organization is thought to facilitate nuclear processes by efficiently reducing the search volume of transcriptional regulators for their cognate DNA elements (19). This principle may also apply to transcription-coupled NER by a mechanism that pre-positions DNA repair enzymes in transcriptionally active chromatin regions via association with nuclear matrix.

The congenital diseases of the *Xeroderma pigmentosum* (XP) complex (XPA–XPG) are characterized by biochemical deficiencies in NER (for review, see ref. 21). XPG syndrome exhibits deficiency in NER, skin sun sensitivity and, in some patients, pronounced developmental and neurological defects (22). These diverse manifestations may reflect involvement of certain XP proteins in DNA repair that is tightly linked to transcription (for review, see ref. 4). Our laboratory and others (23–29) have cloned, sequenced, and biochemically characterized the XPG endonuclease gene. There is now clear evidence that XPG endonuclease performs the specific 3′-side incision ≈5 bp from the photodamaged nucleotides (30). By using a β-galactosidase (β-gal) reporter system, we recently established that nuclear localization signals are responsible for the delivery of XPG into the nucleus (31). We report here that by indirect immunofluorescence detection, cellular XPG endonuclease shows dynamic regulation of its intranucleus distribution within 2 h after a moderate UV-C dose (10 J/m^2). This dynamic does not reflect a detection artifact of the XPG antigenic epitope, as the dynamic was reproduced quantitatively with β-gal fusion protein containing the XPG C-terminal peptides. XPG endonuclease association with the nuclear matrix taken together with its remarkable intranuclear UV dynamics, suggest a testable model in which dynamics of key

Abbreviations: β-gal, β-galactosidase; NER, nuclear excision repair; HSF, human skin fibroblasts.

*M.S.P. and J.A.K. contributed equally to this work.
†To whom reprint requests should be addressed at: Life Sciences Division, M888, Los Alamos National Laboratory, Los Alamos, NM 87545. e-mail: park@telomere.lanl.gov.
‡Present address: University of Cincinnati, Medical Sciences Building, Room 5564, 231 Bethesda Avenue, Cincinnati, OH 45267.

The publication costs of this article were defrayed in part by page charge payment. This article must therefore be hereby marked "*advertisement*" in accordance with 18 U.S.C. §1734 solely to indicate this fact.

enzyme(s) regulates relative NER rates in the active and bulk inactive compartments of the cell nucleus.

MATERIALS AND METHODS

Cells. HeLa S3 cells, human skin fibroblasts HSF-42 (32), and a human Epstein–Barr virus-transformed lymphoblastoid line TK-6 (33) were kindly provided by David Chen and Richard Okinaka (both at Los Alamos National laboratory). HeLa and HSF-42 were maintained in Dulbecco's modified Eagle's medium plus 10% fetal calf serum (FCS, HyClone). TK-6 was cultured in RPMI 1640 medium containing 10% FCS.

Antibody Preparation. The keyhole limpet hemocyanin-conjugated synthetic peptide (34), which was derived from the predicted amino acid sequence SSSDSDDDGGKEKMVLV (aa 1147–1163), was used as the antigen into rabbits. Anti-XPG1322 polyclonal antibodies were purified by a combination of protein G and antigen-affinity columns prepared by succinoamide chemistry. A peptide (aa 747–801) of XPG, which was produced in *Escherichia coli*, was used to immunize mice. The serum collected from the immunized mice was further purified on affinity columns and the antibody was named anti-XPGHLH.

Indirect Immunofluorescence Microscopy. HeLa and HSF-42 cells were grown in chamber slides (Nunc) and processed for immunofluorescence. Cells were washed with ice-cold phosphate-buffered saline (PBS), permeabilized, and fixed by successive incubation in methanol and acetone for 5 min each at −20°C. The cells were incubated in a blocking solution (3% BSA in PBS) for 30 min at 4°C. XPG protein was detected by the combination of anti-XPG1322 and fluorescein-conjugated anti-rabbit IgG. Cells were then analyzed by epifluorescence microscopy (Axioskop, Zeiss) or confocal microscopy. For confocal microscopic analysis, optical sections of 0.5 μm were obtained using a Zeiss confocal laser scanning microscope (LSM-10) equipped with a ×100, 1.4-n.a. objective lens, and an argon ion laser (488 nm). The fluorescence signal was pseudocolored and the image was recorded directly from the screen by photography with Kodachrome 200 film. Images were acquired for quantitative immunofluroescence measurement using a Photometrics (Tucson, AZ) slow-scan cooled CCD camera containing a 1000 × 1000 grade 1 Kodak KAF-1400 chip. The camera was mounted on a Zeiss Axiophot microscope fitted with a standard Zeiss no. 9 filter and a 20× Neufluor dry objective. Images of three to five fields of cells, containing 5 to 20 cells each, were taken from each slide by an investigator who was unaware of the treatment conditions. Images were analyzed using the public domain image analysis software NIH IMAGE (version 1.54, from the National Institutes of Health, Bethesda).

Immunoprecipitation and Immunoblot Analysis. Total nuclear proteins from TK-6 cells (5×10^8) were prepared from the purified nuclei. To immunoprecipitate XPG protein associated with the nuclear matrix, a highly purified nuclei preparation was subjected to further fractionation of nuclear protein. The nuclei were incubated for 10 min at room temperature in nuclei treatment buffer (50 mM Tris·HCl, pH 7.6/4.5 mM $MgCl_2$/100 mM NaCl) with 0.1 mM $CaCl_2$ per 100 mg of DNase per ml per 10 mg of RNase A per ml. Nuclease treated nuclei were pelleted at 500 × *g* for 10 min at 4°C. The pellet was washed 3× in low salt buffer (10 mM Hepes, pH 7.9/2.5 mM $MgCl_2$/20 mM KCl/1.0 mM phenylmethylsulfonyl fluoride/1.0 μg/ml leupeptin/1 mM pepstatin/0.05 units/ml aprotinin) and extracted twice for 15 min on ice in high salt buffer with varying concentrations of NaCl (0.2-2.0 M NaCl/10 mM Hepes, pH 7.9/0.2 mM $MgCl_2$/1.0 mM phenylmethylsulfonyl fluoride/1.0 μg/ml leupeptin/1 mM pepstatin/0.05 units/ml aprotinin). The XPG was immunoprecipitated from the extracts with anti-XPGHLH and protein-G agarose (35), and immunoblotted with anti-XPG1322 (36).

UV Irradiation. Monolayer cultures growing on chamber slides were irradiated with a GE germicidal lamp at a dose of 0.5 J/m²/sec by methods described (23). Immediately after irradiation, prewarmed medium was added to the slides and further incubated for varying times before processing for indirect immunofluorescence studies. At each time point, slides were fixed in methanol and acetone, and stored at −20°C until all slides were collected and further processed as described earlier.

Quantitative Immunofluorescence to Measure the Effects of UV Irradiation on XPG Protein. The effects of UV irradiation on the relative amount and subnuclear distribution of XPG protein were measured in HSF-42 cells at several times after irradiation with 10 J/m², which resulted in the post-UV survival of 45% (M.S.P., unpublished observation). The intensity of immunofluorescence, representing the relative amount of XPG protein, was measured from a digital image of each nucleus. Using the trace tool of the NIH IMAGE program, an area of the cell corresponding to the nucleoplasm was encircled. The mean fluorescence intensity of the pixels inside the trace was then recorded. The mean fluorescence intensity was recorded from at least 50 independent nuclei residing in five isolated areas on a prepared slide. From the same images, density slices were made and the numbers of foci in each nucleus were counted and recorded. For each image/field of cells, the same density slice criteria were used. Signals with a minimum area of four pixels were counted as individual foci.

One-way statistical analysis of variance was done using the VAX/VMS version of MINITAB, release 7.2 (Minitab, State College, PA). Post hoc comparisons were made using Duncan's multiple range test.

The Effects of UV Irradiation on Subnuclear Distribution of XPG Protein. The effects of UV irradiation on the subnuclear distribution of XPG protein was tested by counting the number of the XPG-specific foci in the nucleus. HSF-42 cells were irradiated with 10 J/m² and incubated for various periods of time and were subjected to indirect immunofluorescence microscopy. Then, the numbers of foci with distinct fluorescence signals were recorded from the same nuclei that were used for measuring the total nuclear intensity. The foci that had distinct fluorescent signals with areas equivalent to a minimum of four pixels were counted as individual foci.

Construction of the β-Gal-XPG(aa 1146–1185) Fusion Protein. The C terminus of XPG gene, which contains a putative nuclear localization signal (aa 1171–1185), was synthesized by polymerase chain reaction and fused in single or tandem copies to β-gal in a reporter vector pCH110 (Pharmacia) in frame for proper expression of the fusion proteins under the simian virus 40 (SV40) promoter (37).

Indirect Immunofluorescence Microscopy of β-Gal–XPG Fusion Proteins. HeLa cells were transfected by the calcium phosphate precipitation method (38). Briefly, 2.5×10^4 cells were plated into single-well chamber slides (Nunc) and transfected with 5 μg of plasmid DNA. At 24 h after glycerol shock or at indicated time points, the cells were washed three times with ice-cold PBS and then fixed in ethanol at −20°C for 10 min and subjected to indirect immunofluorescence microscopy with a mouse monoclonal anti-β-gal (1:500 dilution, Sigma, catalog no. G8021) and a fluorescein-conjugated goat anti-mouse IgG (1:250 dilution, Jackson ImmunoResearch).

Immunofluorescence microscopy and confocal microscopy were performed as described for XPG protein. The confocal images were visualized and pseudocolored with the NIH IMAGE program.

The Effects of UV Irradiation on Subnuclear Distribution of β-Gal–XPG Fusion Proteins. The effects of UV irradiation on the subnuclear distribution of the fusion protein (see *Results*) with two copies of XPG(aa 1146–1185) [XPG(aa

1146–1185) × 2] was tested by transfecting HeLa cells as described above with minor changes. Twenty-four hours after the glycerol shock, cells were washed three times with 37°C PBS and then irradiated with 10 J/m^2, which resulted in the post-UV survival of 53% (M.S.P., unpublished observation). The cells were incubated for indicated time periods, and then processed for indirect immunofluorescence analysis. The changes in subnuclear distribution of the β-gal–[XPG(aa 1146–1185) × 2] fusion protein represented as percentiles of the total nuclear fusion protein immunofluorescence associated with the perinucleoli and other foci (here collectively termed "foci"). This percentage was determined from a digital image of a confocal slice through the widest diameter of each nucleus. Using the trace tool with these images we determined the total fluorescence in the nucleus (Nuc_T) and the total fluorescence in the nucleus subtracting that of the foci (Nuc_t). The percentage of the fusion protein associated with the foci was then calculated using the following equation: % of nuclear β-gal in foci = $100 - [(Nuc_t/Nuc_T) \times 100]$.

RESULTS

XPG Fractionation with the Nuclear Matrix. XPG protein was detected using Western blot analysis of nuclear extracts from human lymphoblastoid (TK6) cells. In these experiments standard conditions were used for the isolation of nuclear matrix-associated proteins (39). Efficient solublization of XPG protein from nuclei followed by detection on immunoblots required combined treatments with DNase, RNase, and/or high salt concentration (note the absence of XPG detection without these treatments in Fig. 1, lane 1). DNase I and RNase independently extracted the XPG protein from the nuclear matrix. However, the efficiency of extraction was not as good as the combination of the two nucleases. This may be due to the inherent affinity of XPG to nucleic acids (29). Following pretreatments with nucleases, most of the XPG protein was subsequently eluted from the nuclear pellets with a salt concentration of at least 0.5 M NaCl (Fig. 1, lanes 2–8). This result indicated that the XPG protein is bound fairly tightly, but not integrally, to this preparation. 2 M NaCl concentrations are normally needed to dissociate integral nuclear-matrix structural proteins. For example, nuclear lamin protein required 2 M NaCl extraction to solubilize (data not shown).

Immunofluorescence Localization of XPG Within the Nucleus. The distribution of XPG protein-specific antibody was visualized using epifluorescence (see Fig. 3) and confocal microscopy of human fibroblast cells (HSF-42) (Fig. 2). The

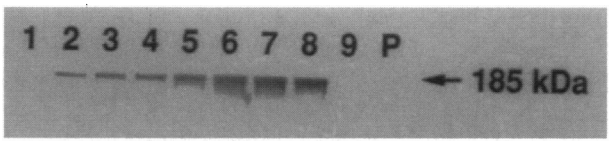

FIG. 1. Immunoprecipitation of XPG protein released from the nucleus of human lymphoid culture (TK-6) by extraction with varying concentrations of NaCl. Lanes: 1, nuclei treated with nuclear matrix treatment buffer without nucleases; 2–8, nuclei treated with nuclear matrix treatment buffer with nucleases and varying concentration of salts, 0.1, 0.2, 0.3, 0.4, 0.5, 1.0, and 2.0 M NaCl, respectively; 9, total lysate of the nucleus after extraction with 2.0 M NaCl.

XPG-specific antibody stains punctate intranuclear structures strongly. Optical sectioning (≈0.5 μm steps) of a typical HSF-42 cell using confocal microscopy indicated that the distribution of intense XPG stained foci was random throughout the depth of the nucleus.

Redistribution of XPG Protein After UV Irradiation. The punctate or focal nuclear localization of XPG protein suggested that it was partially compartmentalized in the absence of DNA damage. Would XPG therefore change in distribution after UV irradiation? In UV-irradiated cells (10 J/m^2), we observed that the XPG immunofluorescence signal became more evenly distributed in the nucleus. Representative HSF-42 cells are shown in Fig. 3, before and at 1 and 2 h after UV. Apparent foci numbers dropped 2- to 3-fold in this time interval. Between 8 and 24 h post-UV, the foci again increased in number.

To more accurately quantify the redistribution of XPG immunofluorescence, the number of distinct foci were counted in digitized images of cell nuclei subjected to UV irradiation (10 J/m^2). At least 50 independent nuclei were blind-counted from either sham-treated or UV-irradiated cells cultured for time intervals from 0.5 h to 24 h after irradiation (Table 1). Analysis of variance revealed highly significant differences in the data ($F = 26.66, df = 6, 359; P < 0.001$). At each time point after UV irradiation, the mean number of foci per nucleus was lower than control. At 1 h post-UV, the average number of foci per nuclei decreased by one-half. By 2 h after irradiation, the mean number of foci per nucleus was five times less than nonirradiated controls (Table 1). By 8 h post-UV, we quantified the reappearance of about 76% of control foci numbers in nuclei sampled. It is important that during the 24 h postirradiation growth time, the mean total fluorescence in nuclei did not show corresponding changes (Table 1).

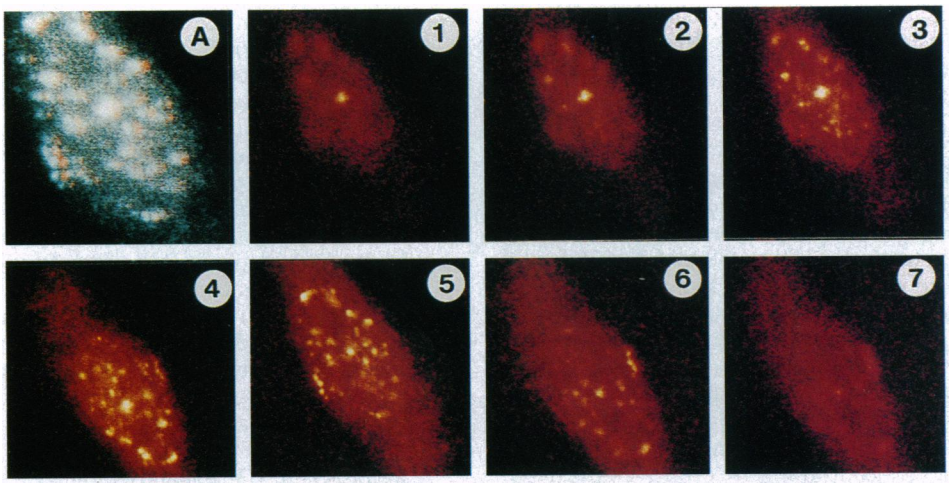

FIG. 2. Confocal microscopic images of XPG protein in the nucleus. Human skin fibroblast cells (HSF-42) were stained with anti-XPG1323 polyclonal antibody and the fluorescein-conjugated goat anti-rabbit IgG. For confocal microscopic analysis, seven optical sections at 0.5 μm increments were obtained (1–7). (*A*) A reconstructed total three-dimensional image of nucleus stained with anti-XPG1322.

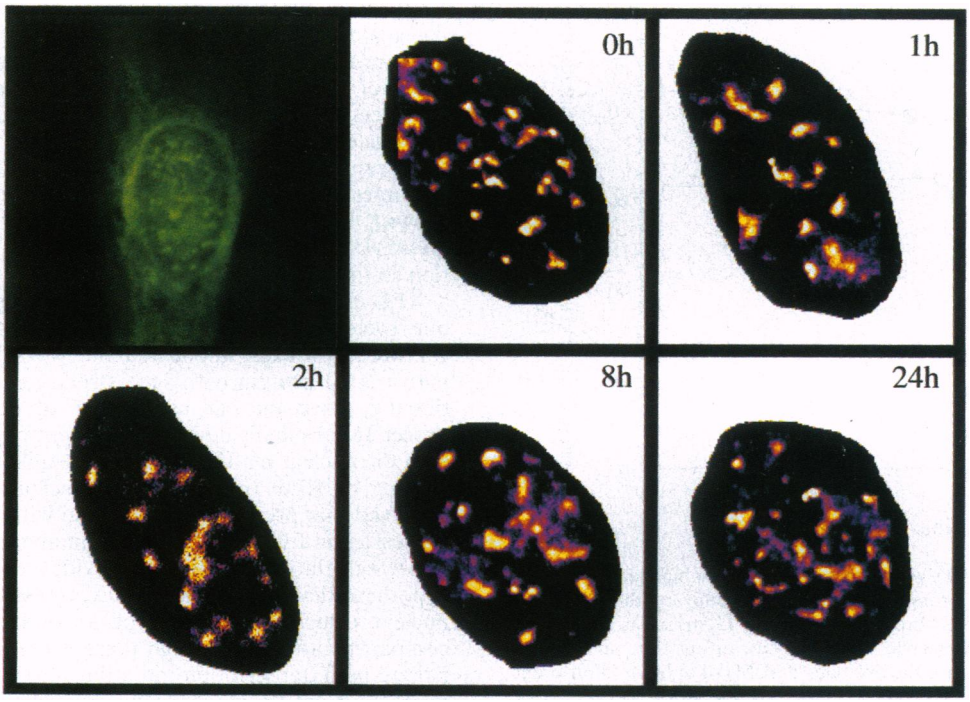

FIG. 3. Nuclear immunofluorescence foci of XPG protein after UV irradiation (10 J/m^2). A representative nucleus of HSF cells from each time point was selected. The images were composited using the NIH IMAGE program.

At this point, we considered an alternative interpretation that XPG dynamics reflected simply a change in epitope accessibility in the XPG protein after UV, rather than physical redistribution of XPG. To evaluate this alternative, we examined the nuclear localization of β-gal fusion proteins containing segments of XPG but detected with a monoclonal antibody to a β-gal epitope.

UV Dynamics of a β-Gal Fusion Protein Containing a C Terminus Peptide of XPG. Transiently expressed β-gal–XPG fusion protein containing the C terminus peptide of XPG (AA 1146–1185) localized completely into the nucleus of human HeLa cells (data not shown). A derivative of that construct, β-gal–[XPG(aa 1146–1185) × 2] fusion protein contained a tandem, in frame, duplication of the C terminus peptide. This fusion protein exhibited complete localization to subnuclear structures, including many foci, and also prominently to the periphery of the nucleolus (Fig. 4). Epifluorescence and confocal microscopy both showed the predominant perinucleolar staining of this protein (Fig. 4 *A* and *B*). Further, confocal optical sectioning of representative HeLa cell nuclei revealed many foci of β-gal staining, outside of the nucleoli (Fig. 4 *B–E*). This observation was similar to the distribution of native XPG protein as extensive foci (but not perinucleolar staining) in normal fibroblasts (Figs. 2 and 3), and in HeLa cells (data not shown). It was quite remarkable to find the β-gal–[XPG(aa 1146–1185) × 2] fusion protein localized to many distinct foci as well as the perinucleolar regions.

We then examined UV effects on the intranuclear distribution of this β-gal–[XPG(aa 1146–1185) × 2] fusion protein. Our fluorescence quantification methods were modified to measure relative immunofluorescence intensities in perinucleolar regions vs. the entire nucleus, in the digitized confocal optical images, as described in the *Materials and Methods*. In Fig. 5, the normalized relative antigenic signal intensities associated with perinucleolar structures were ≈30% of total nuclear fluorescence intensity before UV (data not shown). Following UV exposure (10 J/m^2), the dispersion of β-gal signal to the rest of the nucleus reached a maximum within 2 h postirradiation (Fig. 5). About 60% of the control immunofluorescence signal was reassociated with the perinucleolar regions by 6 h post-UV in the surviving cells (Fig. 5). For comparison, XPG immunofluorescence redistribution data given previously in Table 1 are replotted in Fig. 5.

Table 1. Redistribution of nuclear XPG protein immunofluorescence after UV-irradiation (10 J/m^2)

Time	Mean total nuclear intensity* (±SEM)	Mean XPG foci number† (±SEM)	Relative XPG foci number (% of Control)
0	190 (2.27)	21.2 (1.66)	100
0.5	200 (1.22)	17.1 (1.04)	81
1.0	191 (1.93)	10.7 (0.87)	51
2.0	195 (1.85)	4.4 (0.56)	21
4.0	203 (1.60)	16.1 (0.74)	76
8.0	199 (1.25)	16.5 (0.60)	78
24	202 (0.73)	17.8 (1.20)	84

*Number of nuclei scored >50 per time point.
†Number of nuclei scored >35 per time point.

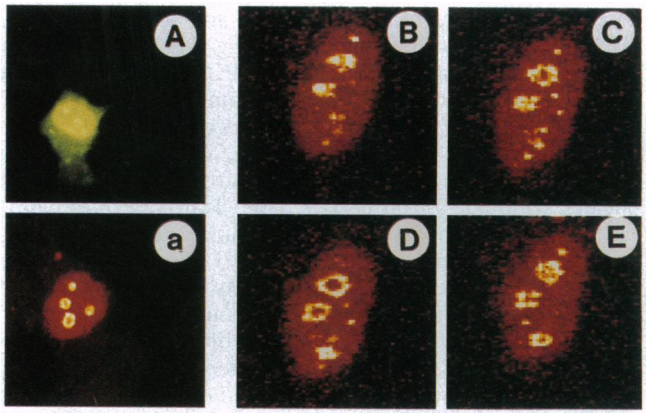

FIG. 4. Subnuclear localization of the β-gal fusion protein with a tandem copy of the XPG(aa 1146–1185). The subnuclear distribution of the fusion protein in HeLa cells was examined by epifluorescence microscopy (*A*) or confocal microscopy using 0.5 μm sectioning from the top of cells (*a, B–E*).

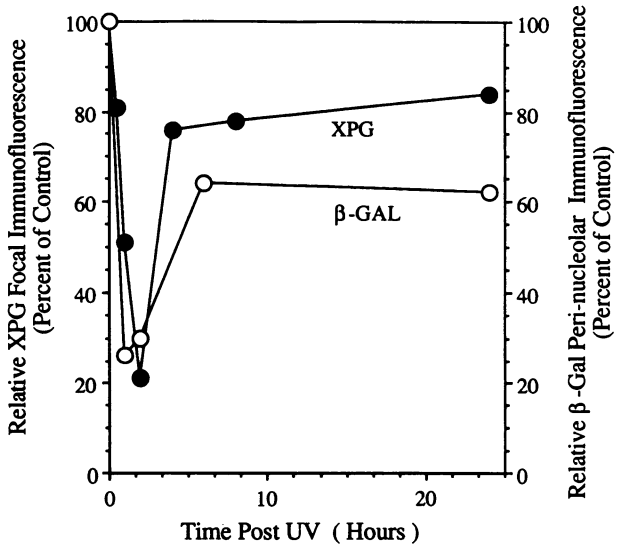

FIG. 5. Effects of UV on the association with subnuclear structures of the β-gal fusion protein with a tandem copy of the XPG (aa 1146–1185). HeLa cells were irradiated with 10 J/m^2 and processed for indirect immunofluorescence microscopy at various time points after irradiation. Numbers are the average (±SEM) of at least 15 different cells from a minimum of two independent transfection experiments for each time point. SEM error bars are smaller than the figure symbols. For comparison, XPG immunofluorescence redistribution data given in Table 1 are replotted.

DISCUSSION

We describe evidence of dynamic and reversible nuclear localization of an essential DNA excision repair enzyme. Specific immunofluorescence of XPG endonuclease is normally localized within the nucleus, and predominantly to a limited number of foci, in human cells. By using a β-gal reporter system, we have previously established that nuclear localization signals are responsible for the delivery of XPG into the nucleus (31). Within 2 h post-UV, XPG foci became dispersed for a brief interval, and therefore greatly reduced in number in digitized epifluorescence images. This redistribution is almost completely reversed within 8 h. Our results have also largely ruled out the possibility that these dynamics are an artifact of variation in XPG epitope detectability by antibody. The alternative possibility is that epitope(s) of XPG may be generally accessible only in foci, but through conformational changes after UV irradiation become more accessible to the antiserum. The β-gal expression experiments point strongly to physical movement of XPG protein after UV irradiation. We have mimicked the focal localization and further the XPG dynamical behavior following UV using β-gal fusion protein containing only a tandem duplicated XPG, C terminus peptide (aa 1146–1185). A monoclonal antiserum to β-gal was used in these experiments. These results provided striking corroboration of a simple model in which native XPG protein diffuses from pre-positioned regions to a more dispersed locale in the nucleus within 1–2 h after UV. The β-gal–[XPG(aa 1146–1185) × 2] fusion protein also localized adventitiously to perinucleolar regions, unlike native XPG. We believe that this is caused by some sequence similarity of the C terminus peptide to nucleolar binding protein motifs (40). Although perinucleolar binding is not seen with XPG, our results indicate that the XPG C-terminal region is itself controlling the dynamics following UV, rather than through changes in a specific binding partner, since localization of the XPG and β-gal–[XPG(aa 1146–1185) × 2] proteins are targeted to heterologous chromatin sites. This was further supported by the fact that neither the formation of foci or perinucleolar binding was observed when β-gal was fused to other regions of XPG that contain potential nuclear localization signals (31). An analogous focal localization of the DNA synthesis protein—proliferating cell nuclear antigen—specifically during S phase of the cell cycle, and its dispersion after UV exposure have been reported (41). Dynamic localization of proliferating cell nuclear antigen was associated specifically with foci of DNA replication. In contrast, the reversible XPG localization dynamics is seen here for mostly G_1 interphase cells (data not shown). Immunofluorescence studies of other XP proteins, notably XPA and XPB, gave no indication of strong localization to intranuclear foci (42, 43).

XPG endonuclease is retained within the nucleus by a tight but reversible association with nuclear structures. Our confocal studies already implicated the reversible association of native XPG protein with such structures, possibly transcriptionally active nuclear matrix. By adopting a biochemical procedure originally developed to identify proteins associated with the nuclear matrix (39), we were able to demonstrate the binding of XPG protein to this nucleus fraction. We also observed that pretreatment of nuclei with DNase and RNase was essential for solubilization of immunoreactive XPG protein by salt elution. These lines of evidence strongly support the hypothesis that XPG protein is directly associated with specific nuclear structure. We do not know the function of this compartmentation, although there is evidence for XPG participation in transcription-initiation complex–TFIIH (44). Immunofluorescence evidence for colocalization of these components is not yet available. We suggest that compartmentation of XPG in actively transcribed regions would readily facilitate NER in active chromatin.

A number of studies have suggested that nuclear matrix associations and chromatin superstructure change during NER (45, 46). Furthermore, the time course of the present XPG dynamics is also consistent with rapid, overall changes in chromatin structure following UV (for review, see ref. 47). Transcriptionally active DNA is also found closely associated with the nuclear matrix (48). Since chromatin containing transcriptionally active DNA sequence is more susceptible to digestion by DNase I, it is reasonable to presume that this DNA is more accessible for DNA repair enzymes as well.

NER proceeds with heterogeneous rates within the nucleus architecture (see ref. 4 and references therein). Interaction of lesions directly with RNA polymerase II complexes, particularly TFIIH, which also contains some bound XPG endonuclease, may be required for preferential repair of transcribed genes in eukaryotes. As there is fairly rapid NER for certain lesions but not others in the bulk chromatin (6, 7, 49), one must assume that a significant fraction of XPG endonuclease is not sequestered in foci. XPG protein concentration is presumed initially concentrated in transcriptionally active, nuclear matrix-bound regions over that found in the general nucleus. A tight association of this critical NER enzyme with active chromatin structures could preferentially alleviate UV-induced inhibition of mRNA transcription, an immediate cause of cell cytotoxicity (50). At the biochemical level, the colocalization of XPG endonuclease within actively transcribed regions would hypothetically result in greater initial velocity of repair incisions in that part of the genome. This scheme is consistent with previous observations. Mullenders *et al.* (14) observed that an initial nonrandom chromatin distribution of NER DNA synthesis was most pronounced directly after UV irradiation, and changed to a more random chromatin distribution after 2 h. This observation also supports the hypothesis that redistribution of DNA repair originates from the nuclear matrix attached region and spreads to other areas of the genome. We are proposing the first molecular model to explain this phenomenon in positing that XPG endonuclease distribution may regulate relative NER rates in the transcriptionally active and inactive nuclear compartments. Elucidation of spatial and temporal movement of XPG will further our

understanding of the complexity of NER at cellular level. Evidently, XPG function(s) could be regulated by its dynamical movement within the nuclear superstructure.

1. Sancar, A. (1994) *Science* **266,** 1954–1956.
2. Huang, J.-C., Svoboda, D. L., Reardon, J. T. & Sancar, A. (1992) *Proc. Natl. Acad. Sci. USA* **89,** 3664–3668.
3. Svoboda, D. L., Taylor, J.-S., Hearst, J. E. & Sancar, A. (1993) *J. Biol. Chem.* **268,** 1931–1936.
4. Bohr, V. A., Phillips, D. H. & Hanawalt, P. C. (1987) *Cancer Res.* **47,** 6426–6436.
5. Hanawalt, P. C. (1994) *Science* **266,** 1957–1958.
6. Bohr, V. A., Smith, C. A., Okumoto, D. S. & Hanawalt, P. C. (1985) *Cell* **40,** 359–369.
7. Mellon, I., Bohr, V., Smith, C. A. & Hanawalt, P. C. (1986) *Proc. Natl. Acad. Sci. USA* **83,** 8878–8882.
8. Schaeffer, L., Roy, R., Humbert, S., Moncollin, V., Vermeulen, W., Hoeijmakers, J. H. J., Chambon, P. & Egly, J.-M. (1993) *Science* **260,** 58–63.
9. Feaver, W. J., Svejstrup, J. Q., Bardwell, L., Bardwell, A. J., Buratowsky, S., Guylas, K. D., Donahue, T. F., Friedberg, E. C. & Kornberg, R. D. (1993) *Cell* **75,** 1379–1387.
10. Drapkin, R., Reardon, J., Ansari, A., Huang, J.-C., Zawel, L., Ahn, K., Sancar, A. & Reinberg, D. (1994a) *Nature (London)* **368,** 769–772.
11. Jackson, D. A., Bass-Hassan, A., Errington, R. J. & Cook, P. R. (1994) *J. Cell Sci.* **107,** 1753–1760.
12. Verheijen, R., Venrooij, W. V. & Ramaekers, F. (1988) *J. Cell Sci.* **90,** 11–36.
13. Hozak, P., Hassan, A. B., Jackson, D. A. & Cook, P. R. (1993) *Cell* **73,** 361–373.
14. Mullenders, L. H. F., van Zeeland, A. A. & Natarajan, A. T. (1983) *Biochim. Biophys. Acta* **740,** 428–435.
15. Jackson, D. A., Balajee, A. S., Mullenders, L. & Cook, P. R. (1994) *J. Cell Sci.* **107,** 1745–1752.
16. Jackson, D. A., Hassan, A. B., Errington, R. J. & Cook, P. (1993) *EMBO J.* **12,** 1059–1065.
17. Xing, Y., Johnson, C. V., Dobner, P. R. & Lawrence, J. B. (1993) *Science* **259,** 1326–1133.
18. Carter, K. C., Bowman, D., Carrington, W., Fogarty, K., McNeil, J. A., Fay, F. C. & Lawrence, J. B. (1993) *Science* **259,** 1330–1335.
19. Cockerill, P. N. & Garrad, W. T. (1986) *Cell* **44,** 273–282.
20. Razin, S. V., Kekelidze, M. G., Lakanidin, E. M., Scherrer, K. & Georgiev, G. P. (1986) *Nucleic Acids Res.* **14,** 8189–8207.
21. Cleaver, J. E. & Kraemer, K. H. (1989) in *Metabolic Basis of Inherited Disease*, eds. Scriver, C. R., Beauder, A. L., Sly, W. S. & Valle, D. (McGraw–Hill, New York), pp. 2949–2971.
22. Vermeulen, W., Jaeken, J., Jaspers, N. G., Bootsma, D. & Hoeijmakers, J. H. J. (1993) *Am. J. Hum. Genet.* **53,** 185–192.
23. MacInnes, M. A., Dickson, J. A., Hernandez, R. R., Learmonth, D., Lin, G. Y., Mudgett, J. S., Park, M. S., Shauer, S., Reynolds, R. J., Strniste, G. F. & Yu, J. Y. (1993) *Mol. Cell. Biol.* **13,** 6393–6402.
24. Scherly, D., Nouspikel, T., Corlet,, Ucla, C., Bairoch, C. A. & Clarkson, S. G. (1993) *Nature (London)* **363,** 182–185.
25. Shiomi, T., Harada, Y., Saito, T., Shiomi, N., Okuno, Y. & Yamaizumi, M. (1994) *Mutat. Res.* **314,** 167–175.
26. O'Donovan, A. & Wood, R. D. (1993) *Nature (London)* **363,** 185–188.
27. O'Donovan, A., Scherly, D., Clarkson, S. G. & Wood, R. (1994) *J. Biol. Chem.* **269,** 15965–15968.
28. Habraken, Y., Sung, P., Prakash, L. & Prakash, S. (1994) *Nucleic Acids Res.* **22,** 3312–3316.
29. Cloud, K., Shen, B., Strniste, G. F. & Park, M. S. (1995) *Mutat. Res.* **347,** 55–60.
30. O'Donovan, A., Davies A., A., Moggs, J. G., West, S. C. & Wood, R. D. (1994) *Nature (London)* **371,** 432–435.
31. Knauf, J. A., Pendergrass, S. H., Marrone, B. L., Strniste, G. F., MacInnes, M. A. & Park, M. S. (1996) *Mutat. Res.* **363,** 67–75.
32. Chen, D. J., Strniste, G. F. & Tokita, N. (1984) *Radiat. Res.* **100,** 321–327.
33. Skopek, T. R., Liber, H. L., Penman, P. W. & Thilly, W. G. (1978) *Biochem. Biophys. Res. Commun.* **84,** 4767–4771.
34. Green, N., Alexander, H., Olson, A., Alexander, S., Shinnick, T. M., Sutcliffe, M. & Lerner, R. A. (1982) *Cell* **28,** 477–488.
35. Springer, T. A. (1989) in *Current Protocols in Molecular Biology*, eds. Ausubel, F. M., Brent, R., Kingston, R. E., Moore, D. D., Seidman, J. G., Smith, J. A. & Struhl, K. (Green, New York), pp. 10.16.1–10.16.11.
36. Blake, M. S., Johnston, K. H., Russell-Jones, G. J. & Gotschlich, E. C. (1984) *Anal. Biochem.* **136,** 175–179.
37. Schreiber, V., Molinete, M., Boeuf, H., de Murcia, G. & Menissier-de Murcia, J. (1992) *EMBO J.* **11,** 3263–3269.
38. Graham, F. L. & van der Eb, A. J. (1973) *Virology* **52,** 456–467.
39. Fey, E. G., Wan, K. M. & Penman, S. (1984) *J. Cell Biol.* **98,** 1973–1984.
40. Yan, C. & Melese, T. (1993) *J. Cell Biol.* **123,** 1081–1091.
41. Celis, J. E. & Madsen, P. (1986) *J. Cell Sci.* **209,** 277–283.
42. Miyamoto, I., Miura, N., Niwa, H., Miyazaki, J. & Tanaka, K. (1992) *Proc. Natl. Acad. Sci. USA* **89,** 12182–12187.
43. Ma, L., Westbroek, A., Jochemsen, A. G., Weeda, G., Bosch, A., Bootsma, D., Hoeijmakers, J. H. J. & van der Eb, A. J. (1994) *Mol. Cell. Biol.* **14,** 4126–4134.
44. Mu, D., Park, C.-H., Matsunaga, T., Hsu, D. S., Reardon, J. T. & Sancar, A. (1995) *J. Biol. Chem.* **270,** 2415–2418.
45. Mullenders, L. H. F., van Kesteren, A. C., Bussmann, C. J. M., van Zeeland, A. A. & Natarajan, A. T. (1986) *Carcinogenesis* **7,** 995-1002.
46. Mullenders, L. H. F., van Kesteren van Leeuwen, A. C., van Zeeland, A. A. & Natarajan, A. T. (1988) *Nucleic Acids Res.* **16,** 10607–10622.
47. Smerdon, M. J. (1989) in *DNA Repair Mechanisms and Their Biological Implications in Mammalian Cells*, eds. Lambert, M. W. & Laval, J. (Plenum, New York), pp. 271–294.
48. Ciejek, E. M., Tsai, M. J. & O'Malley, B. W. (1983) *Nature (London)* **306,** 607–609.
49. Mitchell, D. L., Brash, D. E. & Nairn, R. S. (1990) *Nucleic Acids Res.* **18,** 963–971.
50. Bohr, V. A., Okumoto, D. S. & Hanawalt, P. C. (1986) *Proc. Natl. Acad. Sci. USA* **83,** 3830–3833.